PCCP

Accepted Manuscript

This is an *Accepted Manuscript*, which has been through the Royal Society of Chemistry peer review process and has been accepted for publication.

Accepted Manuscripts are published online shortly after acceptance, before technical editing, formatting and proof reading. Using this free service, authors can make their results available to the community, in citable form, before we publish the edited article. We will replace this *Accepted Manuscript* with the edited and formatted *Advance Article* as soon as it is available.

You can find more information about *Accepted Manuscripts* in the Information for Authors.

Please note that technical editing may introduce minor changes to the text and/or graphics, which may alter content. The journal's standard Terms & Conditions and the Ethical guidelines still apply. In no event shall the Royal Society of Chemistry be held responsible for any errors or omissions in this *Accepted Manuscript* or any consequences arising from the use of any information it contains.

ROYAL SOCIETY OF CHEMISTRY

www.rsc.org/pccp

1 **Unraveling the mechanism of 720 nm sub-band-gap optical absorption of Ta_3N_5**
2 **semiconductor photocatalyst: a hybrid-DFT calculation**
3
4 Jiajia Wang,[ab] Aibin Ma,[*ac] Zhaosheng Li,[*b] Jinghua Jiang,[ac] Jianyong Feng[b] and
5 Zhigang Zou[b]
6
7 [a] *College of Mechanics and Materials, Hohai University, Nanjing 210098, China.*
8 [b] *National Laboratory of Solid State Microstructures, Department of Physics,*
9 *Ecomaterials and Renewable Energy Research Center (ERERC), and College of*
10 *Engineering and Applied Sciences, Nanjing University, Nanjing 210093, People's*
11 *Republic of China.*
12 [c] *Jiangsu collaborative innovation center of advanced micro/nano materials &*
13 *equipment, Nanjing 210094, China.*
14
15
16
17
18
19
20
21 * Corresponding Authors: Tel: +86-25-83787239, Fax: +86-25-83786046.
22 E-mail:aibin-ma@hhu.edu.cn(A.B. MA) or zsli@nju.edu.cn(Z. S. Li)

Physical Chemistry Chemical Physics Accepted Manuscript

1 **Abstract:** The Ta_3N_5 semiconductor photocatalyst possesses a 720 nm (about 1.72 eV)
2 sub-band-gap optical absorption but the mechanism of this optical absorption is still
3 controversial. In this study, the hybrid density functional theory calculations are
4 performed to unravel the mechanism of 720 nm sub-band-gap optical absorption of
5 Ta_3N_5. By study of possible optical absorptions initiated by the O_N impurity and V_N
6 defect, we find that the 720 nm sub-band-gap optical absorption of Ta_3N_5 may be
7 ascribed to the electrons transition from $V_N^{\bullet}$ to $V_N^{\bullet\bullet\bullet}$. In addition, we propose that the
8 720 nm sub-band-gap optical absorption can be used to qualitatively evaluate the
9 photocatalytic water splitting ability of Ta_3N_5.

10
11
12
13
14
15
16
17
18
19
20
21
22

Physical Chemistry Chemical Physics Accepted Manuscript

1 **1. Introduction**

2 Optical properties of semiconductors are very important for understanding and utilizing
3 their functional properties. For semiconductor-based photocatalysts, the optical
4 properties are especially important because realizing visible light response is
5 fundamental for an ideal photocatalyst. In order to absorb the visible portion of solar
6 light as much as possible, the optical band gap of photocatalyst should be about 2.0 eV.
7 Among various semiconductor photocatalysts, the tantalum nitride (Ta_3N_5)
8 semiconductor has recently attracted a great of interest because of its excellent
9 performance in the photocatalytic water splitting[1-5]. Due to appropriate optical band gap
10 (about 2.1 eV) and band edges positions, the theoretic maximum solar-to-hydrogen
11 efficiency of Ta_3N_5 is as high as 15.9%[6], suggesting that Ta_3N_5 is one potential
12 semiconductor photocatalyst to split water into H_2 and O_2.

13 Although Ta_3N_5 has been extensively studied from experiments[2-5] and theoretical
14 calculations[7-10], most work associated with Ta_3N_5 has focused on improving its
15 photocatalytic activity and chemical stability, while some problems associated with the
16 optical properties of Ta_3N_5 remain to be resolved. Fig. 1 shows the schematic optical
17 absorption spectrum of Ta_3N_5. It can be seen that, besides the 590 nm (about 2.1 eV)
18 band gap optical absorption, the Ta_3N_5 also has a sub-band-gap optical absorption
19 around 720 nm (about 1.72 eV)[11,12]. The 590 nm band gap optical absorption is ascribed
20 to electron excitation from the valence band maximum (VBM) to the conduction band
21 minimum (CBM), while the origin of 720 nm sub-band-gap optical absorption is still
22 controversial. Some work attributes the 720 nm sub-band-gap optical absorption to

Physical Chemistry Chemical Physics Accepted Manuscript

Physical Chemistry Chemical Physics Accepted Manuscript

trapping and de-trapping of conduction band electrons at the neutral and reduced Ta centers[11,13,14], other work attributes the 720 nm sub-band-gap optical absorption to nitrogen vacancy (V_N) that forms during prolonged nitridation of Ta_3N_5 samples[12]. Unfortunately, none of the above two explanations of the 720 nm sub-band-gap optical absorption has been experimentally or theoretically verified.

In this study, the hybrid density functional theory (DFT) calculations are performed to unravel the mechanism of 720 nm sub-band-gap optical absorption of Ta_3N_5. To our knowledge, the sub-band-gap optical absorption and optical emission of semiconductors are usually correlated with various defects in semiconductors, but an in-depth understanding of defects, especially the charged defects in Ta_3N_5 is still inadequate so far. In Ta_3N_5, the V_N is the major intrinsic defect because anion vacancies such as nitrogen vacancy and oxygen vacancy are usually the most common defects in metal nitrides and oxides. However, both experimental[15,16] and theoretical[7,8] investigations have proved that the substitution of oxygen for nitrogen (O_N) is another most important impurity in Ta_3N_5. Note that, although the nominal constitutional elements of Ta_3N_5 are only composed of Ta and N, the practical Ta_3N_5 samples naturally consist of considerable amounts of O_N impurities, which may come from the residual O of Ta_2O_5 precursor after nitridation treatment. Furthermore, despite of various experimental conditions, the O_N impurities cannot be completely eliminated from Ta_3N_5[15,16]. The O_N impurity has an important effect on the optical properties of Ta_3N_5, because the optical band gaps of O_N-doped Ta_3N_5 are oxygen-concentration dependent[17]. With the increase of O_N concentrations, the optical band gap of O_N-doped Ta_3N_5 first

Physical Chemistry Chemical Physics Accepted Manuscript

1 decreases and then increases, agreeing well with the experimental observations[16]. Our
2 recent theoretical calculations reveal that the O_N impurities help stabilize Ta_3N_5
3 surfaces[8] and maintain mechanical stability[9] of Ta_3N_5, validating that the natural
4 existence of O_N impurity is theoretically favorable in Ta_3N_5. Therefore, besides the
5 intrinsic V_N defect, the O_N impurity is also properly correlated with the 720 nm
6 sub-band-gap optical absorption and must be considered in this study.
7

8 **2. Computational methodology**

9 The hybrid-DFT calculations are performed using the VASP[18] code, implemented with
10 the projector augmented wave (PAW[19]) method. The Hyde-Scuseria-Ernzerhof (HSE[20])
11 hybrid functional, which is good at reproducing the accurate electronic structures of
12 semiconductors, is adopted for the hybrid-DFT calculations. The accuracy of HSE
13 functional is determined by two critical parameters, α and ω, which are the fraction of
14 semilocal Perdew-Burke-Ernzerhof (PBE[21]) functional replaced by a screened nonlocal
15 functional and the inverse screening length, respectively. In our calculations, α and ω
16 are 25% and 0.2 $Å^{-1}$, respectively, which refer to the HSE06[22] functional. For N, O and
17 Ta, the $2s^22p^3$, $2s^22p^4$ and $5p^65d^46s^1$ orbital, respectively, are treated as the valence
18 states. The cutoff energy for basis functional is 400 eV. Geometry relaxations are
19 performed until the residual forces on each ion converged to be smaller than 0.02 eV $Å^{-1}$.
20 Based on the above computational parameters, the calculated band gap of pure Ta_3N_5 is
21 2.2 eV, which is close to the experimental band gap of Ta_3N_5 (about 2.1 eV). The
22 relaxed lattice constants of pure Ta_3N_5 are a=3.87, b=10.25 and c=10.27 Å, which are

Physical Chemistry Chemical Physics Accepted Manuscript

1 also in good agreement with the experimental values (a=3.89, b=10.21 and c=10.26
2 Å)[23].
3 The inset in Fig. 1 shows the conventional cell of bulk Ta_3N_5. The Ta atom is
4 coordinated with six neighboring N atoms, while N atoms are coordinated with three or
5 four Ta atoms. Since both experiments[16] and theoretical calculations[8] have proved that
6 the 3-coordinated N atom is easily substituted by O atom, only the 3-coordinated N
7 atom is removed and substituted by one O atom to build Ta_3N_5 with V_N (denoted as
8 $Ta_3N_5+V_N$) and O_N-doped Ta_3N_5 (denoted as $Ta_3N_5+O_N$), respectively. We construct a
9 3×1×1 (11.61×10.25×10.27 Å^3) Ta_3N_5 supercell which contains 60 N and 36 Ta atoms.
10 Doping with one O_N impurity into this supercell corresponds to about 1.7% doping
11 concentration, which is in agreement with the about 5% O_N concentration in
12 experiments[15,16]. Due to the large supercell size and rather time-consuming HSE
13 calculations, only one Gamma centered *k*-point is used for the Brillouin zone integration.
14 However, this does not affect the reliability of our calculated results because (a) the
15 same *k*-point set is also adopted for the HSE calculations of the TaON[24] supercell which
16 has nearly the same cell sizes as the Ta_3N_5 supercell in this study, and (b) we recalculate
17 some critical results with a dense 2×2×2 *k*-point meshes (8 *k*-points) to ensure the
18 reliability of our results.
19
20 **3. Results and discussion**
21 **3.1 Electronic structures**
22 We firstly calculate the density of states (DOS) to study electronic structures of charged

1 O_N and charged V_N in Ta_3N_5. For comparison purpose, the DOS of pure Ta_3N_5 is also
2 calculated and shown in Fig. 2a. The O_N impurity can be theoretically presented in the
3 neutral ($Ta_3N_5 + O_N^{\times}$ in Fig. 2b) and singly positive ($Ta_3N_5 + O_N^{\bullet}$ in Fig. 2c) charge
4 states. Comparisons between Fig. 2a and 2b reveal that, the CBM of $Ta_3N_5 + O_N^{\times}$
5 shifts left compared with that of pure Ta_3N_5. Integral DOS of the left shift part of CBM
6 is one, suggesting that one electron is localized at the CBM of $Ta_3N_5 + O_N^{\times}$. Partial
7 charge density of the CBM of $Ta_3N_5 + O_N^{\times}$ (Fig. 2h) further reveals that this electron is
8 uniformly distributed only on Ta atoms, indicating that the neutral Ta ($Ta_{Ta}^{\times}$) atoms in
9 $Ta_3N_5 + O_N^{\times}$ are reduced by electrons donated from $O_N^{\times}$. Note that, although the
10 valence state of reduced Ta can not be precisely determined, the reduced Ta hereinafter
11 is expressed by singly negative ($Ta_{Ta}^{'}$) charged state. This is merely for the convenience
12 of discussion and will not affect any qualitative analyses in this study. In $Ta_3N_5 + O_N^{\bullet}$,
13 where the electron donated from $O_N^{\times}$ is removed, the $Ta_{Ta}^{'}$ returns to the neutral
14 $Ta_{Ta}^{\times}$ state which is essentially equal to the CBM position. Since the Ta atom is no
15 longer reduced, the left shift of CBM disappears in $Ta_3N_5 + O_N^{\bullet}$ and the DOS of
16 $Ta_3N_5 + O_N^{\bullet}$ becomes almost the same as that of pure Ta_3N_5.

17 The above DOS results reveal that, in O_N-doped Ta_3N_5, the $O_N^{\times}$ can be
18 qualitatively regarded as the combination of one $O_N^{\bullet}$ and one $Ta_{Ta}^{'}$. This means that,
19 the variation of O_N valence states, *i.e.*, the electron transition between $O_N^{\times}$ and $O_N^{\bullet}$, is
20 merely trapping and de-trapping of conduction band electrons at the $Ta_{Ta}^{\times}$ and $Ta_{Ta}^{'}$
21 centers. In addition, the above DOS results also provide a proper explanation to the poor
22 H_2 evolution ability of Ta_3N_5. Experiments[2,25] reveal that, although Ta_3N_5 is

Physical Chemistry Chemical Physics Accepted Manuscript

Physical Chemistry Chemical Physics Accepted Manuscript

1 theoretically an excellent photocatalyst, its practical H_2 evolution ability is poor. Since
2 the CBM position of one semiconductor reflects its reduction ability to split water into
3 H_2, the more negative CBM position of $Ta_3N_5 + O_N^\times$ suggests that the O_N impurity is
4 one possible source of the poor H_2 evolution ability of Ta_3N_5.

5 Compared with the O_N impurity, the V_N defect is able to donate up to three
6 electrons to the lattice of Ta_3N_5. Then, the V_N defect can be theoretically presented in
7 the neutral ($Ta_3N_5 + V_N^\times$ in Fig. 2d), singly positive ($Ta_3N_5 + V_N^\bullet$ in Fig. 2e), doubly
8 positive ($Ta_3N_5 + V_N^{\bullet\bullet}$ in Fig. 2f) and triply positive ($Ta_3N_5 + V_N^{\bullet\bullet\bullet}$ in Fig. 2g) charge
9 states. In $Ta_3N_5 + V_N^\times$, where three electrons are donated from $V_N^\times$, there is a defect
10 state in the band gap. Integral DOS of this defect state is two, indicating that two of the
11 three electrons are localized in the in-gap defect state. Partial charge density of this
12 in-gap defect state (Fig. 2i) shows that these two electrons are mainly localized in the
13 V_N site. The left one electron is localized at the CBM of $Ta_3N_5 + V_N^\times$ and induces the
14 left shift of CBM, suggesting that the V_N defect is another possible source of the poor
15 H_2 evolution ability of Ta_3N_5. Partial charge density of the CBM of $Ta_3N_5 + V_N^\times$ (Fig.
16 2j) reveals that this electron is uniformly distributed only on Ta atoms, indicating that
17 the $V_N^\times$ defect is also able to reduce the Ta atoms from $Ta_{Ta}^\times$ to $Ta_{Ta}^{'}$. In
18 $Ta_3N_5 + V_N^\bullet$, where one electron is removed, the in-gap defect state and the
19 corresponding partial charge density (Fig. 2k) are not changed but the left shift of CBM
20 disappears. In $Ta_3N_5 + V_N^{\bullet\bullet}$, where two electrons are removed, the defect state remains
21 in the band gap but only one electron is localized in the V_N site (Fig. 2l). If all the three
22 electrons are removed, the in-gap defect state disappears from the band gap of

1 $Ta_3N_5 + V_N^{\bullet\bullet\bullet}$.

2 The above DOS results reveal that, similar to the O_N impurity, the $V_N^{\times}$ can also be
3 qualitatively regarded as the combination of one $V_N^{\bullet}$ and one $Ta_{Ta}^{'}$. Then, the electron
4 transition between $V_N^{\times}$ and $V_N^{\bullet}$ is still trapping and de-trapping of conduction band
5 electrons at the $Ta_{Ta}^{\times}$ and $Ta_{Ta}^{'}$ centers. When the V_N valence states vary between
6 $V_N^{\bullet}$ and $V_N^{\bullet\bullet}$ (or $V_N^{\bullet\bullet\bullet}$), electrons in the in-gap defect state will participle in the
7 electron transition.

8

9 **3.2 Thermodynamic properties**

10 Although O_N and V_N can be theoretically presented in different valence states, some
11 valence states of O_N and V_N may be thermodynamically unstable. Therefore, we
12 secondly calculate formation energies of the charged O_N and charged V_N to study
13 whether O_N and V_N in all charge states are thermodynamically stable. The formation
14 energy of defect α in charge state q is calculated using the following equation[26]:

15 $$E_f(\alpha,q) = E_t(\alpha,q) - E_t(host) + \sum n_i \Delta\mu_i + q(\varepsilon_F + \Delta V) \qquad (1)$$

16 where $E_t(\alpha,q)$ and $E_t(host)$ are total energies of Ta_3N_5 supercell with the defect α
17 in charge state q and that without defect in the neutral charge state, respectively, n_i is
18 the number of constituent i (i=N, O, Ta), $\Delta\mu_i$ is the chemical potential of constituent i
19 referenced to the total energy per atom of its pure elemental phase (bulk Ta, O_2 gas and
20 N_2 gas), ε_F is the Fermi energy level referenced to the VBM, and ΔV is a correction
21 to align the reference potential in the defective supercell with that in defect-free
22 supercell.

Physical Chemistry Chemical Physics Accepted Manuscript

Physical Chemistry Chemical Physics Accepted Manuscript

1 Due to the finite size supercell and charged defects, the image charge correction
2 proposed by Makov-Payne[27] should be calculated in this study. The image charge
3 correction generally contains monopole and quadrupole corrections. Unfortunately, due
4 to the non-cubic cell shape of Ta_3N_5 supercell, only the monopole correction can be
5 correctly calculated by the VASP code. Therefore, only the monopole correction is
6 calculated for the image charge correction in this study. However, this will not affect
7 our calculated results because the quadrupole correction is typically ~30% of the
8 monopole correction[28]. This treatment of image charge correction is also adopted in
9 other theoretical work[24].

10 As can be seen in Eqn. (1), the defect formation energy depends on the chemical
11 potential $\Delta\mu_i$. To ensure the reliability of defect formation energies, the $\Delta\mu_i$ must be
12 carefully calculated. Under thermal equilibrium growth conditions, Ta_3N_5 should
13 satisfy:

14 $$3\Delta\mu_{Ta} + 5\Delta\mu_N = E^f_{Ta_3N_5} = -9.39eV \quad (2)$$

15 where $E^f_{Ta_3N_5}$ is the formation energy of the pure Ta_3N_5. $\Delta\mu_i$=0 (i=N, Ta) represents
16 the limit where the element is so rich that the pure elemental phases will form.
17 Therefore, to avoid formation of the pure elemental phases in Ta_3N_5, $\Delta\mu_i$<0 must be
18 satisfied. Then, based on Eqn. (2), the $\Delta\mu_N$ and $\Delta\mu_{Ta}$ under different growth
19 conditions can be determined: under N-poor growth condition, $\Delta\mu_N$=-1.88 and
20 $\Delta\mu_{Ta}$=0 eV; under N-rich growth condition, $\Delta\mu_N$=0 and $\Delta\mu_{Ta}$=-3.13 eV. In the
21 O_N-doped Ta_3N_5, to avoid the precipitation of secondary phases such as Ta_2O_5 and
22 TaON, as well as the pure O_2 gas, the following inequations should be satisfied

1 simultaneously:

2 $$5\Delta\mu_O + 2\Delta\mu_{Ta} < E^f_{Ta_2O_5} = -18.59eV$$

3 $$\Delta\mu_N + \Delta\mu_O + \Delta\mu_{Ta} < E^f_{TaON} = -6.26eV \qquad (3)$$

4 $$\Delta\mu_O < 0$$

5 where $E^f_{Ta_2O_5}$ and E^f_{TaON} are formation energies of Ta_2O_5 and TaON, respectively.
6 Then, the $\Delta\mu_O$ under N-poor and N-rich growth conditions are -4.38 and -3.12 eV,
7 respectively.

8 Using the above chemical potentials, the defect formation energies of charged O_N
9 and charged V_N are calculated and shown in Fig. 3a and 3b, respectively. Fig. 3a reveals
10 that both $O_N^{\times}$ and $O_N^{\bullet}$ are thermodynamically stable. Fig. 3b reveals that, except $V_N^{\bullet\bullet}$,
11 the $V_N^{\times}$, $V_N^{\bullet}$ and $V_N^{\bullet\bullet\bullet}$ are thermodynamically stable. This means that the V_N defect
12 in Ta_3N_5 behaves as a negative-*U*[29] center which is also found in some metal oxides
13 with anion defects, for example the oxygen vacancy in ZnO[30] is a negative-*U* center. Fig.
14 3 also reflects the thermodynamic transition levels[26] of O_N and V_N. The thermodynamic
15 transition level $\varepsilon_\alpha(q/q')$ is the Fermi energy level ε_F at which the formation energy
16 of defect α in charge state *q* is equal to that of the same defect but in charge state q'.
17 Since both O_N and V_N are electron donors in Ta_3N_5, the thermodynamic transition levels
18 of O_N and V_N are also called the ionization energies[26]. Fig. 3a and 3b show that
19 $\varepsilon_{O_N}(0/+1)$ and $\varepsilon_{V_N}(0/+1)$ are as low as 0.06 and 0.16 eV (below the CBM),
20 respectively, suggesting that both $O_N^{\times}$ and $V_N^{\times}$ in Ta_3N_5 are shallow donors. In other
21 words, the thermodynamic electron transition between 0 and +1 charge state is easily for
22 both O_N and V_N. Since the above DOS results reveal that, for O_N and V_N, the electron

Physical Chemistry Chemical Physics Accepted Manuscript

Physical Chemistry Chemical Physics Accepted Manuscript

1 transition between 0 and +1 charge state is essentially trapping and de-trapping of
2 electrons at the $Ta_{Ta}^{\times}$ and $Ta_{Ta}^{'}$ centers, the small ionization energies of $O_{N}^{\times}$ and $V_{N}^{\times}$
3 may be ascribed to the easily electron transition between $Ta_{Ta}^{\times}$ and $Ta_{Ta}^{'}$.
4

5 **3.3 Optical properties**

6 Based on the in-depth understanding of electronic structures and thermodynamic
7 properties of the charged O_N and charged V_N in Ta_3N_5, we finally calculate possible
8 optical absorptions initiated by the O_N and V_N centers to unravel the mechanism of 720
9 nm sub-band-gap optical absorption of Ta_3N_5. Before studying the optical properties of
10 Ta_3N_5, it is worthwhile to make a discussion of the optical transition mechanism in the
11 defective semiconductors.

12 Using a defect D in the $q1$ and $q2$ ($q1<q2$) charge states as an example, Fig. 4
13 shows the schematic diagram of optical transitions for the defect doped semiconductor.
14 It can be seen that, the optical transitions between D^{q1} and D^{q2} involve with two
15 possible optical absorptions and two possible optical emissions. One optical absorption
16 occurs through the process $D^{q1}+h\nu \rightarrow D^{q2}+\mathrm{e}$ in which D^{q1} absorbs a photon and is
17 converted to D^{q2} with an electron at the CBM (Fig. 4a). After geometry relaxation, the
18 D^{q2} is relaxed to the ground state. Then, the optical emission process occurs when the
19 electron at the CBM is recombined with the hole trapped at D^{q2} (Fig. 4b). The other
20 possible optical absorption occurs through the process $D^{q2}+h\nu \rightarrow D^{q1}+\mathrm{h}$ in which D^{q2}
21 accepts an electron excited from the VBM and is converted to D^{q1}, with a hole (h)
22 trapping at the VBM (Fig. 4c). The optical emission process occurs when the electron in

1 D^{q1} is recombined with the hole trapped at the VBM (Fig. 4d). The optical absorption
2 energy in Fig. 4a and optical emission energy in Fig. 4b can be derived from the
3 following Eqn. (4a) and (4b), respectively[26,31]:

4 $$\varepsilon^{opt}(D^{q1}/D^{q2}) = E^{f}(D^{q2}/D^{q1}) - E^{f}(D^{q1}/D^{q1}) \quad (4a)$$

5 $$\varepsilon^{opt}(D^{q2}/D^{q1}) = E^{f}(D^{q2}/D^{q2}) - E^{f}(D^{q1}/D^{q2}) \quad (4b)$$

6 where $E^{f}(D^{x}/D^{y})$ (x,y=q1 or q2) denotes formation energy of D^{x} with the relaxed
7 geometry of D^{y}. The optical absorption energy in Fig. 4c and optical emission energy in
8 Fig. 4d can be calculated by the similar method. It is worthy of mentioning that, the
9 optical transition level is defined similar to but actually different from the
10 thermodynamic transition level calculated in the Section 3.2. More details of the optical
11 transition level, as well as the differences between optical transition level and
12 thermodynamic transition level, can be found in Ref. 26.

13 Fig. 5 shows the possible optical absorption and optical emission energies initiated
14 by O_N and V_N centers in the form of configuration coordinated diagram[26]. It can be seen
15 that:

16 (i) In Fig. 5a and 5b, the optical absorption energies $\varepsilon^{opt}(O_N^{\times}/O_N^{\bullet})$ and
17 $\varepsilon^{opt}(O_N^{\bullet}/O_N^{\times})$ are 0.10 (12400 nm) and 2.16 (574 nm) eV, respectively, which are in
18 disagreement with the 720 nm sub-band-gap optical absorption. The optical absorption
19 in Fig. 5a corresponds to the optical transition mechanism in Fig. 4a. Since the electron
20 transition between $O_N^{\times}$ and $O_N^{\bullet}$ corresponds to that between $Ta_{Ta}^{'}$ and $Ta_{Ta}^{\times}$ (equal
21 to the CBM position), the 0.10 eV optical absorption energy initiated from $O_N^{\times}$ to $O_N^{\bullet}$
22 is attributed to the electron excitation from $Ta_{Ta}^{'}$ to CBM, which needs a very small

Physical Chemistry Chemical Physics Accepted Manuscript

Physical Chemistry Chemical Physics Accepted Manuscript

1 energy because Ta'_{Ta} just locates at the bottom of CBM. The optical absorption in Fig.
2 5b corresponds to the optical transition mechanism in Fig. 4c. The 2.16 eV optical
3 absorption energy initiated from $O_N^{\bullet}$ to $O_N^{\times}$ is attributed to the electron excitation
4 from VBM to $Ta_{Ta}^{\times}$. Since $Ta_{Ta}^{\times}$ is equal to the CBM position, the 2.16 eV optical
5 absorption occurs through the electron excitation from VBM to CBM, which is nearly
6 equal to the band gap of Ta_3N_5;
7 (ii) In Fig. 5c and 5d, the optical absorption energies $\varepsilon^{opt}(V_N^{\times}/V_N^{\bullet})$ and
8 $\varepsilon^{opt}(V_N^{\bullet}/V_N^{\times})$ are 0.21 (5905 nm) and 2.07 (599 nm) eV, respectively, which are not
9 equal to the 720 nm sub-band-gap optical absorption. Since the electron transition
10 between $V_N^{\times}$ and $V_N^{\bullet}$ is also trapping and de-trapping of electrons at the $Ta_{Ta}^{\times}$ and
11 Ta'_{Ta} centers, the optical transition mechanisms between $V_N^{\times}$ and $V_N^{\bullet}$ is similar to
12 that between $O_N^{\times}$ and $O_N^{\bullet}$. This is also the reason why both the optical absorption and
13 optical emission energies in Fig. 5c and 5d are close to that in Fig. 5a and 5b,
14 respectively;
15 (iii) In Fig. 5e and 5f, the optical absorption energy $\varepsilon^{opt}(V_N^{\bullet}/V_N^{\bullet\bullet\bullet})$ and
16 $\varepsilon^{opt}(V_N^{\bullet\bullet\bullet}/V_N^{\bullet})$ are 1.98 (626 nm) and 2.15 (577 nm) eV, respectively. The 1.98 eV (626
17 nm) optical absorption energy is close to 720 nm, suggesting that the 720 nm
18 sub-band-gap absorption of Ta_3N_5 is likely attributable to electrons transition from $V_N^{\bullet}$
19 to $V_N^{\bullet\bullet\bullet}$. After increasing the *k*-point from single Gamma point to the dense 2×2×2
20 *k*-point meshes (8 *k*-points), the recalculated $\varepsilon^{opt}(V_N^{\bullet}/V_N^{\bullet\bullet\bullet})$ is 1.74 eV (713 nm), which
21 is in good agreement with the experimental observed 720 nm sub-band-gap absorption.
22 Although $V_N^{\bullet\bullet}$ is a thermodynamically unstable charge state, we also calculate the

1 optical absorption associated with $V_N^{\bullet\bullet}$. As can be seen in Fig. 5g to 5j, all the four
2 possible optical absorption energies associated with $V_N^{\bullet\bullet}$ are not equal to 1.72 eV (720
3 nm), further confirming that the 720 nm sub-band-gap optical absorption may be
4 ascribed to the electron transition from $V_N^{\bullet}$ to $V_N^{\bullet\bullet\bullet}$.
5 Based on the relationship between V_N defect and 720 nm sub-band-gap optical
6 absorption, we propose that the 720 nm optical absorption can be treated as a fingerprint
7 of the V_N defect in Ta_3N_5. More importantly, since the V_N defect may lower the H_2
8 evolution ability of Ta_3N_5, we can further use the 720 nm optical absorption to
9 qualitatively predict or evaluate the photocatalytic water splitting ability of Ta_3N_5. For
10 example, experiments[11] reveal that, the H_2 evolution ability of Ta_3N_5 with the weak 720
11 nm optical absorption intensity is much better than that with the strong 720 nm optical
12 absorption intensity, which may be ascribed to the less V_N defects in the former Ta_3N_5
13 semiconductor photocatalyst. We hope that the future investigations of the Ta_3N_5
14 semiconductor photocatalyst may be enlightened from this study.
15
16 **4. Conclusions**
17 In summary, based on the hybrid-DFT calculations, we unravel the mechanism of 720
18 nm sub-band-gap optical absorption of Ta_3N_5. By study of possible optical transitions
19 initiated by O_N and V_N centers, we find that the 720 nm sub-band-gap optical absorption
20 may be ascribed to the electron transition from $V_N^{\bullet}$ to $V_N^{\bullet\bullet\bullet}$. Moreover, the electronic
21 structures and thermodynamic properties of the charged O_N and charged V_N have been
22 intensively investigated in this study. This will provide significant indications for future

Physical Chemistry Chemical Physics Accepted Manuscript

1 investigations of the Ta_3N_5 semiconductor photocatalyst.

2

3 **ACKNOWLEDGMENT**

4 This work is supported by National Basic Research Program of China (973 Program,
5 2013CB632404), a Project Funded by the Priority Academic Program Development of
6 Jiangsu Higher Education Institutions, New Century Excellent Talents in University
7 (NCET-12-0268), the National Natural Science Foundation of China (No. 51272102),
8 Natural Science Foundation of Jiangsu Province of China (Grant No. BK20131373) and
9 National Natural Science Foundation of China (Grant No. 51141002). We are also
10 grateful to the High Performance Computing Center (HPCC) of Nanjing University for
11 doing the numerical calculations in this paper on its IBM Blade cluster system.

12

13 **REFERENCES**

14 1. Z. Li, W. Luo, M. Zhang, J. Feng and Z. Zou, *Energ. Environ. Sci.*, 2013, **6**, 347-370.
15 2. M. Hara, G. Hitoki, T. Takata, J. N. Kondo, H. Kobayashi and K. Domen, *Catal. Today*, 2003, **78**,
16 555-560.
17 3. M. Liao, J. Feng, W. Luo, Z. Wang, J. Zhang, Z. Li, T. Yu and Z. Zou, *Adv. Funct. Mater.*, 2012,
18 **22**, 3066-3074.
19 4. M. Li, W. Luo, D. Cao, X. Zhao, Z. Li, T. Yu and Z. Zou, *Angew. Chem. Int. Ed.*, 2013, **52**,
20 11016-11020.
21 5. G. J. Liu, J. Y. Shi, F. X. Zhang, Z. Chen, J. F. Han, C. M. Ding, S. S. Chen, Z. L. Wang, H. X.
22 Han and C. Li, *Angew. Chem. Int. Ed.*, 2014, **53**, 7295-7299.
23 6. A. Murphy, P. Barnes, L. Randeniya, I. Plumb, I. Grey, M. Horne and J. Glasscock, *Int. J.*
24 *Hydrogen Energ.*, 2006, **31**, 1999-2017.
25 7. E. Watanabe, H. Ushiyama and K. Yamashita, *Chem. Phys. Lett.*, 2013, **561**, 57-62.
26 8. J. Wang, W. Luo, J. Feng, L. Zhang, Z. Li and Z. Zou, *Phys. Chem. Chem. Phys.*, 2013, **15**,
27 16054-16064.
28 9. J. Wang, J. Feng, L. Zhang, Z. Li and Z. Zou, *Phys. Chem. Chem. Phys.*, 2014, **16**, 15375-15380.
29 10. M. Harb, P. Sautet, E. Nurlaela, P. Raybaud, L. Cavallo, K. Domen, J.-M. Basseta and K.
30 Takanabe, *Phys. Chem. Chem. Phys.*, 2014, **16**, 20548-20560.
31 11. L. Yuliati, J.-H. Yang, X. Wang, K. Maeda, T. Takata, M. Antonietti and K. Domen, *J. Mater.*

Physical Chemistry Chemical Physics Accepted Manuscript

1 *Chem.*, 2010, **20**, 4295-4298.
2 12. A. Dabirian and R. van de Krol, *Appl. Phys. Lett.*, 2013, **102**, 033905.
3 13. Y. Lee, K. Nukumizu, T. Watanabe, T. Takata, M. Hara, M. Yoshimura and K. Domen, *Chem.*
4 *Lett.*, 2006, **35**, 352-353.
5 14. K. Maeda, N. Nishimura and K. Domen, *Appl. Catal. A*, 2009, **370**, 88-92.
6 15. M. Ritala, P. Kalsi, D. Riihelä, K. Kukli, M. Leskelä and J. Jokinen, *Chem. Mater.*, 1999, **11**,
7 1712-1718.
8 16. S. J. Henderson and A. L. Hector, *J. Solid State Chem.*, 2006, **179**, 3518-3524.
9 17. J. Wang, T. Fang, L. Zhang, J. Feng, Z. Li and Z. Zou, *J. Catal.*, 2014, **309**, 291-299.
10 18. G. Kresse and J. Furthmüller, *Phys. Rev. B*, 1996, **54**, 11169.
11 19. P. E. Blöchl, *Phys. Rev. B*, 1994, **50**, 17953.
12 20. J. Heyd, G. E. Scuseria and M. Ernzerhof, *J. Chem. Phys.*, 2003, **118**, 8207-8215.
13 21. J. P. Perdew, K. Burke and M. Ernzerhof, *Phys. Rev. Lett.*, 1996, **77**, 3865-3868.
14 22. A. V. Krukau, O. A. Vydrov, A. F. Izmaylov and G. E. Scuseria, *J. Chem. Phys.*, 2006, **125**,
15 224106.
16 23. N. E. Brese, M. O'Keeffe, P. Rauch and F. J. DiSalvo, *Acta Crystallogr. Sect. C: Cryst. Struct.*
17 *Commun.*, 1991, **47**, 2291-2294.
18 24. S. Chen and L.-W. Wang, *Appl. Phys. Lett.*, 2011, **99**, 222103.
19 25. D. Lu, M. Hara, T. Hisatomi, T. Takata and K. Domen, *J. Phys. Chem. C*, 2009, **113**,
20 17151-17155.
21 26. C. G. Van de Walle and J. Neugebauer, *J. Appl. Phys.*, 2004, **95**, 3851-3879.
22 27. G. Makov, R. Shah and M. C. Payne, *Phys. Rev. B*, 1996, **53**, 15513-15517.
23 28. C. Persson, Y. J. Zhao, S. Lany and A. Zunger, *Phys. Rev. B*, 2005, **72**, 035211.
24 29. P. W. Anderson, *Phys. Rev. Lett.*, 1975, **34**, 953-955.
25 30. A. Janotti and C. G. Van de Walle, *Appl. Phys. Lett.*, 2005, **87**, 122102.
26 31. P. Reunchan, N. Umezawa, S. Ouyang and J. Ye, *Phys. Chem. Chem. Phys.*, 2012, **14**,
27 1876-1880.
28
29
30
31

Physical Chemistry Chemical Physics Accepted Manuscript

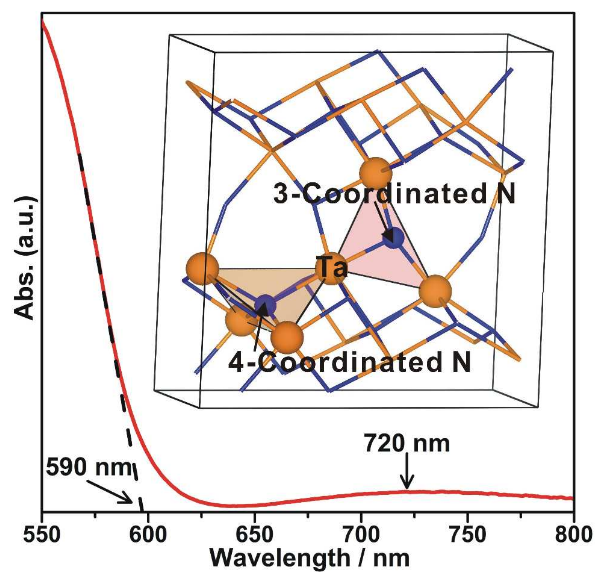

1

2 **Fig. 1** The schematic optical absorption spectrum of the Ta_3N_5 semiconductor. Inset is

3 the conventional cell of the bulk Ta_3N_5.

4

5

6

7

8

Physical Chemistry Chemical Physics Accepted Manuscript

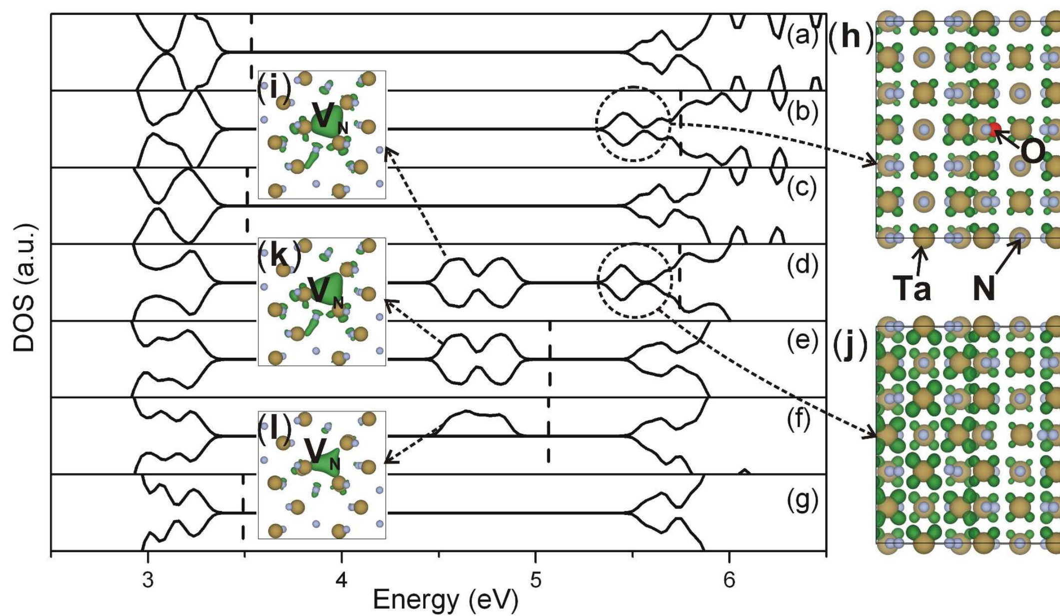

Fig. 2 The DOS of (a) pure Ta_3N_5, (b) $Ta_3N_5 + O_N^{\times}$, (c) $Ta_3N_5 + O_N^{\bullet}$, (d) $Ta_3N_5 + V_N^{\times}$, (e) $Ta_3N_5 + V_N^{\bullet}$, (f) $Ta_3N_5 + V_N^{\bullet\bullet}$ and (g) $Ta_3N_5 + V_N^{\bullet\bullet\bullet}$. In each case, the vertical dash line is the Fermi level. The horizontal axes of (b) to (g) are aligned with that of (a) by the electrostatic potentials. (h) to (l) are partial charge densities of the labeled CBM or in-gap defect state (isosurface level=0.001 electron/Å^3).

Physical Chemistry Chemical Physics Accepted Manuscript

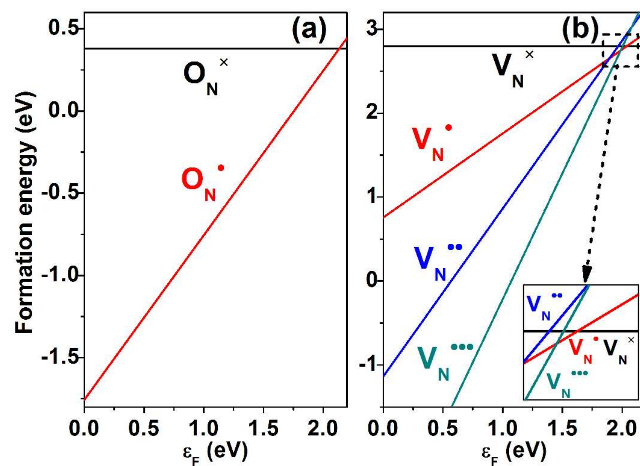

1

2 **Fig. 3** Defect formation energies as a function of the Fermi level (ε_F) for (a) O_N and (b)

3 V_N defects under the N-rich growth condition.

4

5

6

7

8

9

10

11

12

Physical Chemistry Chemical Physics Accepted Manuscript

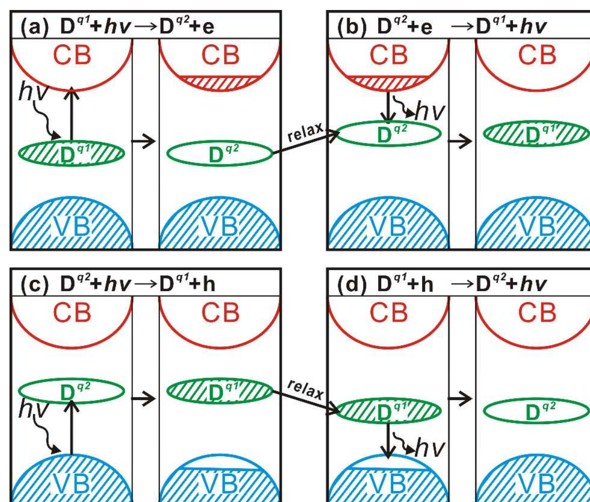

1

2 **Fig. 4** Two optical absorption [(a) and (c)] and two optical emission [(b) and (d)]

3 processes in a semiconductor when the valence states of the defect D vary between $q1$

4 and $q2$ ($q1<q2$) charge state. The shaded and blank areas denote electron occupied and

5 electron unoccupied states, respectively.

6

7

8

9

10

11

Physical Chemistry Chemical Physics Accepted Manuscript

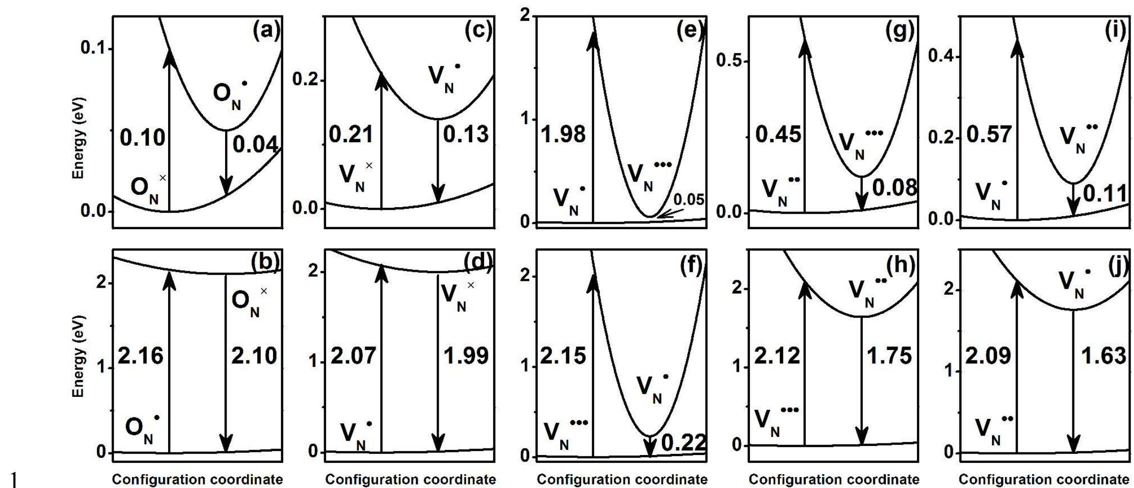

Fig. 5 Calculated configuration coordinate diagram for the O_N [(a) and (b)] and V_N [(c) to (j)] defects in Ta_3N_5. The charged defect formation energies, which are used to obtain the configuration coordinate diagram, are calculated with the Fermi level locating at the CBM and under the N-rich growth condition.

Physical Chemistry Chemical Physics Accepted Manuscript